Counterintuitive energy shifts in joint electron–nuclear-energy spectra of strong-field fragmentation of H_2^+

Zhuo Wang,[1] Min Li,[1,*] Yueming Zhou,[1] Yang Li,[1] Pengfei Lan,[1,†] and Peixiang Lu[1,2]

[1]*School of Physics and Wuhan National Laboratory for Optoelectronics, Huazhong University of Science and Technology, Wuhan 430074, China*

[2]*Laboratory of Optical Information Technology, Wuhan Institute of Technology, Wuhan 430205, China*

By numerically solving the time-dependent Schrödinger equation, we investigate electron–nuclear-energy sharing in strong-field fragmentation of the H_2^+ molecule. We find a counterintuitive energy shift in the joint electron–nuclear-energy spectrum. This energy shift becomes larger for lower nuclear energies. Through tracing the time evolution of the electron wave packet of bound states, we identify that the energy shift originates from the Stark effect due to the coupling of the ground state and the first exited state of the H_2^+ molecule in strong laser fields. We achieve a good agreement between the *ab initio* result and the analytic method that includes the Stark effect of molecules.

I. INTRODUCTION

The interaction of atoms and molecules with an intense laser pulse has been extensively studied. Many interesting strong-field phenomena have attracted attention over the past several decades [1–14], e.g., high-harmonic generation [1–4], molecular dissociation [5–9], Coulomb explosion [10,11], and so on. Compared with atoms, molecules can provide more information about the ionization process because of the additional dimension associated with the multiple centers of the molecular ions. Usually, the electron and nuclear dynamics in molecules are correlated and cannot be analyzed in isolation [15]. For example, in molecular autoionization the lifetime of the autoionizing double-excited states is relatively long, such that the nuclei have enough time to move before the electron is liberated. In this case, the electron and nuclear dynamics are coupled and must be considered on an equal footing [16].

Investigation of the correlated electron-nuclear dynamics can provide deep insight into the mechanism of molecular photonionization and fragmentation. An essential question in the electron-nuclear correlation is how the photon energy is deposited to the electron and nuclei during the laser-molecule interaction. Theoretically, this issue has been extensively studied for strong-field fragmentation of the H_2^+ molecule[17–22]. In 2012 Madsen *et al.* [17] introduced the joint energy spectrum (JES) to investigate the strong-field fragmentation process and it is found that clear evidence of electron-nuclear correlation can be visualized in JES for multiphoton dissociative ionization of H_2^+. More recently, an energy-resolved population imaging method is further proposed [20] to study the electron-nuclear correlation. The energy-sharing rule for the correlated electron and nuclei is deduced by demonstrating the temporary population transfer in the vibrational H_2^+ molecule exposed to extreme ultraviolet pulses. Experimental considerations of strong-field fragmentation greatly benefit from the development of the coincident measurement technology [23], with which the electron energy and the ion

energy can be simultaneously measured. Using the coincident measurement method, Wu *et al.* [24] experimentally observed the energy sharing between the emitted electron and nuclei from above-threshold multiphoton dissociative ionization of the H_2 molecule.

Moreover, it is found that the electron-nuclei energy sharing in the tunnel ionization differs from that in the multiphoton regime [18,20]. Electrons don't share energy with the nuclei in the tunneling regime, while electrons resulted from the multiphoton ionization share part of their energy with the nuclei. In the multiphoton regime, the electron–nuclear-energy-sharing rule in the Coulomb explosion process is sketched in Fig. 1. The electron energy and the nuclear energy satisfy [20]

$$E_e = n\omega + V_g - U_p - E_N, \tag{1}$$

in the above-threshold multiphoton ionization. Here, E_e and E_N represent the electronic energy and nuclear energy, respectively. ω, U_p, and V_g denote the laser frequency, ponderomotive energy of the electron due to the presence of the laser field, and potential curve of the ground state, respectively. n is the photon number absorbed in the process.

In this paper, we study the electron–nuclear-energy sharing in strong-field fragmentation of H_2^+ by numerically solving the time-dependent Schrödinger equation (TDSE). By quantitatively analyzing the JES, we revisit the energy sharing rule given by Eq. (1). A counterintuitive energy shift in the JES is found. With the decrease of the nuclear energies, the energy shift increases. By tracing the time evolution of the electron wave packet of bound states, we find that the origin of the energy shift of H_2^+ is the Stark effect induced by the strong coupling of the two lowest-lying states in strong fields. Additionally, we calculate the Stark-induced shift using an analytical method, which is in good agreement with the *ab initio* result.

II. THEORETICAL MODEL

A. The reduced-dimensionality model of H_2^+

In the numerical simulations, we first use the reduced-dimensionality model (one nuclear plus one electronic degree

_____
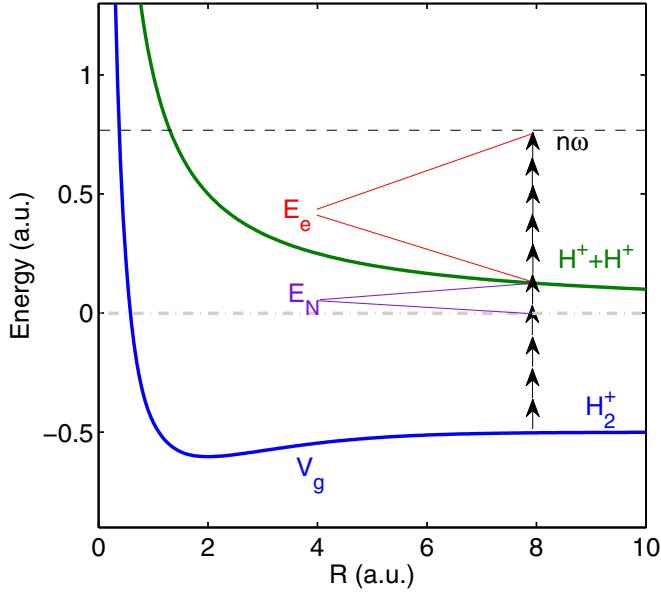
*mli@hust.edu.cn

†pengfeilan@hust.edu.cn

FIG. 1. Illustration of electron–nuclear-energy sharing in the Coulomb explosion process of the H_2^+ molecule.

of freedom) of H_2^+ interacting with an intense linearly polarized pulse [25]. The model can reproduce many experimental results [25,26]. We assumed that the electronic and nuclear motion are restricted along the polarization direction of the pulse which is parallel to the molecular axis. Then, the TDSE can be written as (Hartree atomic units are used throughout unless otherwise indicated)

$$i\frac{\partial}{\partial t}\Psi(R,x;t) = H(x,R;t)\Psi(R,x;t), \qquad (2)$$

where

$$H(x,R;t) = -\frac{1}{2\mu_R}\frac{\partial^2}{\partial R^2} - \frac{1}{2\mu_e}\frac{\partial^2}{\partial x^2}$$
$$- \frac{1}{\sqrt{(x-R/2)^2+\alpha(R)}}$$
$$- \frac{1}{\sqrt{(x+R/2)^2+\alpha(R)}} + \frac{1}{R}$$
$$+ \left(1+\frac{1}{2m_p+1}\right)xF(t). \qquad (3)$$

Here, R is the internuclear distance, x is the electron position measured from the center of mass of the protons, and $\mu_e = 2m_p/(2m_p + 1)$ and $\mu_R = m_p/2$ are the reduced masses with m_p as the mass of the proton. $\alpha(R)$ is the modified soft-core parameter [25], which is adjusted to reproduce the electronic ground-state potential curve. The pulse is defined as $F(t) = F_0 \sin(\pi t/\tau_0)^2 \sin(\omega_0 t)$ being the electric field of the laser pulse. F_0, τ_0, and ω_0 denote the peak electric field amplitude, pulse duration, and angular frequency, respectively. In the simulation, ω_0 and τ_0 are chosen as 0.114 a.u ($\lambda = 400$ nm) and nine optical cycles, respectively. The intensity of the pulse is 9×10^{13} W/cm^2, corresponding to the Keldysh parameter $\gamma = 2.5$.

The TDSE is solved on a grid using the Crank-Nicholson method with a time step of $\delta t = 0.04$ a.u.. We have used a box with $|x| \leqslant 2000$ a.u. and $R \leqslant 25$ a.u., with uniform grid spacings of $\delta x = 0.2$ and $\delta R = 0.05$. The ground state of H_2^+ (electronic $1s\sigma_g$ state and $\upsilon = 15$ state) is chosen to be the initial state of the system and is obtained by propagating the field-free Schrödinger equation in imaginary time. Then, the JES can be obtained by using the method from [18].

B. The frozen nuclei model of H_2^+

We have solved the TDSE for the frozen nuclei model of H_2^+ in order to calculate the electronic above-threshold ionization (ATI) spectrum. In the simulation, we assumed that the nuclei is fixed and the vibrational energy of the nuclei is zero when the Coulomb explosion starts. The electronic TDSE can be written as

$$i\frac{\partial}{\partial t}\Psi(x,t) = H(x,t)\Psi(x,t). \qquad (4)$$

The corresponding Hamiltonian is

$$H(x,t) = -\frac{1}{2}\frac{\partial^2}{\partial x^2} - \frac{1}{\sqrt{(x-R/2)^2+\alpha(R)}}$$
$$- \frac{1}{\sqrt{(x+R/2)^2+\alpha(R)}} + \frac{1}{R} + xF(t). \qquad (5)$$

In the simulation, the x ranges from -800 to 800 a.u. with 16 000 points. To suppress the nonphysical reflection from the simulation border, we introduce a mask function in the boundary.

Finally, the electronic ATI spectrum of H_2^+ can be calculated by applying the energy window operator [27–30],

$$W(\epsilon,k,\eta) = \frac{\eta^{2k}}{(H-\epsilon)^{2k}+\eta^{2k}}. \qquad (6)$$

The probability density of the energy ϵ can be obtained from

$$P(\epsilon) = \frac{\langle\Psi(x)|W|\Psi(x)\rangle}{C}, \qquad (7)$$

with $C = \eta\frac{\pi}{k}\csc(\frac{\pi}{2k})$.

Due to the Coulomb repulsion of the two protons, the nuclear energy can be obtained by the internuclear distance $E_N = 1/R$ in the Coulomb explosion of H_2^+ (assuming that the vibrational energy of the nuclei is zero when the Coulomb explosion starts). In the process, E_e and E_N are correlated through the internuclear distance R. In order to obtain the JES of H_2^+ with fixed internuclear distance R, we have solved the electronic TDSE for many R in the range where $1/R = E_N$ covers the E_N from 0.1 to 0.5 a.u.. Because the electron–nuclear-energy sharing is different in the multiphoton ionization regime and the tunneling regime [18,20], in our simulation, the Keldysh parameter is kept at $\gamma = 2.5$ to make sure that the ionization occurs in the multiphoton regime throughout the calculation. We take a 400-nm laser pulse for discussion to have a large photon energy. The laser intensity
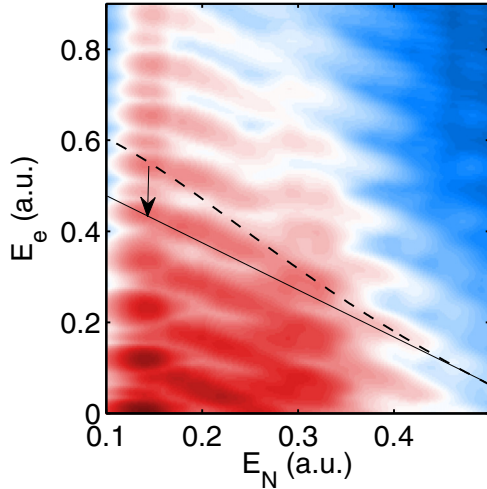
FIG. 2. Electron-nuclear JES for the Coulomb explosion process of H_2^+ ($1s\sigma_g, \upsilon = 15$) in a 400-nm laser pulse by using the method from Ref. [18], where both the nuclei and the electron can move. The intensity is 9×10^{13} W/cm^2 and the pulse duration is nine optical cycles. The dashed curve is obtained by Eq. (1) with $n = 11$. The color scale is logarithmic.

ranges from 8.8×10^{13} to 1.6×10^{14} W/cm^2 corresponding to the nuclear energy changing from 0.1 to 0.5 a.u..

For comparison, a hydrogenlike model atom is chosen. The binding potential of the atom is given by

$$V_x(x) = -\frac{1}{\sqrt{x^2 + b}}, \tag{8}$$

where b is the soft-core parameter. In our simulation, we change the ionization energy I_p of the atom by adjusting the soft-core parameter b. Since the ionization energy of H_2^+

is dependent on the internuclear distance R, the value of the soft-core parameter b is chosen to make sure that the ionization energy of the model atom is the same as that of the H_2^+ molecule. Thus the effect of the ionization potential on the electron energy spectrum is removed.

III. RESULTS AND DISCUSSION

Figure 2 shows the electron-nuclear JES for the Coulomb explosion process of H_2^+ ($1s\sigma_g, \upsilon = 15$) in a 400-nm laser pulse using the method from Ref. [18], where both the nuclei and the electron can move. Two main features are observed: (i) the tilted stripes, which indicated the energy sharing between the electron and nuclei; (ii) the multistripe structure spaced by the photon energy, revealing multiphoton absorption beyond the ionization threshold. We further analyzed the JES quantitatively. The dashed curve in Fig. 2 is obtained by Eq. (1) with $n = 11$. Surprisingly, the peak positions of the JES (guided by the solid line) exhibit obvious energy shifts with respect to the dashed curve, especially for lower nuclear energies. For one stripe, i.e., the peaks absorbing the same number photons for various nuclear energies, it can be seen that as the increase of the nuclear energies, the energy shift (indicated by the arrow) decreases.

Figure 3(a) shows the electron-nuclear JES for the Coulomb explosion process of the H_2^+ molecule obtained by the frozen nuclei model. It can be found that two JESs calculated by two different methods are very similar, especially for the details of the stripes. The energy shifts for the low nuclear energy can be clearly observed in Fig. 3(a), consistent with the observation in Fig. 2. Therefore, our theoretical treatment for the nuclei in the frozen nuclei model is reliable. For simplicity, in the following part, we will use the frozen nuclei model to investigate the origin of the energy shifts in Figs. 2 and 3(a). Figures 3(b)
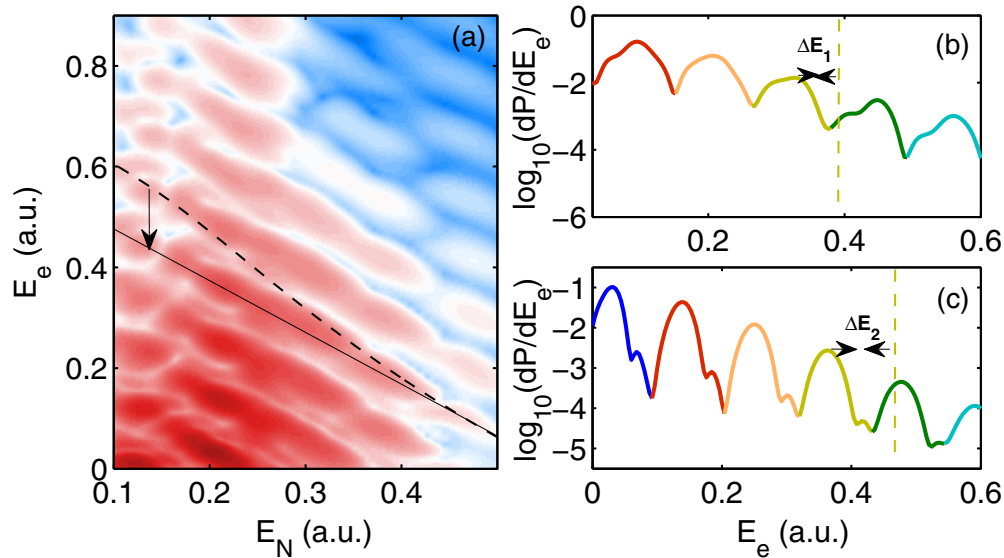

FIG. 3. (a) Electron-nuclear JES for the Coulomb explosion process of H_2^+ obtained by the frozen nuclei model. The dashed curve is obtained by Eq. (1) with $n = 11$. The color scale is logarithmic. (b) and (c) Show the two cuts of (a) for $E_N = 0.25$ a.u. and $E_N = 0.18$ a.u., respectively. The vertical axes are arbitrary units. The peaks with the same color in (b) and (c) represent that the electronic ATI peaks absorbing the same number photons. The vertical dashed lines indicate the electronic energies obtained by Eq. (1). The intensities of the laser field are 1.2×10^{14} and 1×10^{14} W/cm^2 for (b) and (c), respectively.
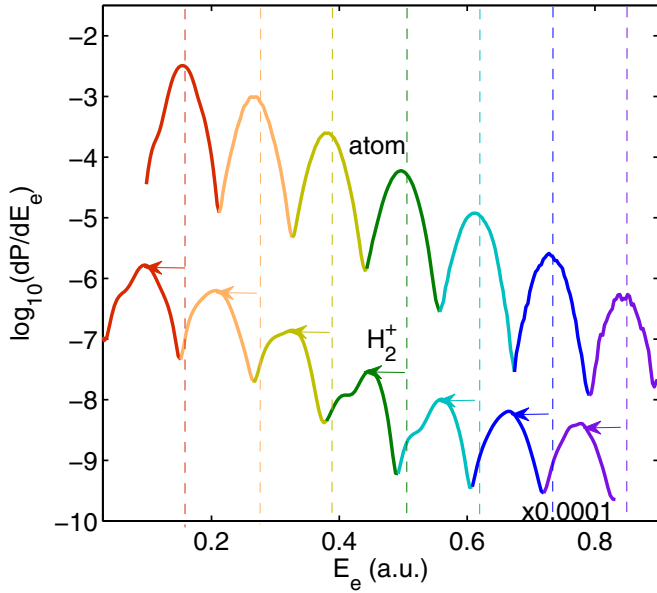
FIG. 4. The electronic ATI spectra on the logarithmic scale and in arbitrary units at $I_p = 0.8$ a.u. for the model atom and H_2^+ molecule, respectively. The vertical dashed lines indicate the electron energies $E_e = n\omega - I_p - U_p$. The peaks of the two spectra, with the same color, denote the ATI peaks with absorbtion of the same number of photons. The laser intensity is 1.2×10^{14} W/cm^2.

and 3(c) show the two cuts of Fig. 3(a) for $E_N = 0.25$ a.u. and $E_N = 0.18$ a.u., respectively. The peaks with the same color in Figs. 3(b) and 3(c) represent the electronic ATI peaks absorbing the same number photons. The vertical dashed lines indicate the electronic energies obtained by Eq. (1). One can clearly see that the energy shift for larger nuclear energy is smaller than the energy shift for smaller nuclear energy, i.e., $\Delta E_1 < \Delta E_2$.

To uncover the origin of the counterintuitive energy shift in the JES for strong-field fragmentation of H_2^+, we compare the electronic ATI spectra of H_2^+ with a hydrogenlike model atom exposed to the same laser pulse. For H_2^+, the cut $E_N = 0.25$ a.u., where $I_p = 0.8$ a.u., is chosen. To remove the effect of the ionization potential, we adjust the soft-core parameter b to make sure that the ionization energy of the atom is the same as that of the H_2^+ molecule. The electronic ATI spectra of the two cases are presented in Fig. 4. The vertical dashed lines indicate the electron energies that are obtained by $E_e = n\omega - I_p - U_p$ [31], where n is the total number of photons in the ionization process. The peaks of the two spectra, with the same color, denote the ATI peaks with absorption of the same number of photons. One can find that the ATI peak position of strong-field ionization of molecules shifts towards lower energy compared with the dashed lines, while this energy shift for the atom is negligible. Therefore, the energy shift in the JES of Fig. 3(a) is related to the molecular structure of H_2^+.

To further show how the electron energy spectrum is influenced by the nuclei, by applying the energy window operator [27–30], we calculate the time evolution of the electron wave packet of the bound states of H_2^+ in nine different nuclear energies. As shown in Figs. 5(a)–5(i), the nuclear energy increases gradually. The color indicates the population density of the bound states. Obviously, all

the bound states energies of H_2^+ oscillate with the evolution of the laser field due to the Stark effect. The bound population appears to spread in the energy direction. This is associated with the window width 2η in the energy window operator. The width of theses curves would decrease with η. Note that the ground state (green dashed curve) and the first excited state (solid curve) of the H_2^+ molecule are degenerate for a very large internuclear distance. The energy gap between the two lowest-lying states becomes larger as the nuclear energy increases, as shown in Fig. 5. Influenced by the Stark effect in the strong fields, the structure of the oscillation of the ground state is consistent with the shape of $-|F(t)|$, while the first excited state exhibits similar oscillatory behavior but towards the opposite direction. Finally, the energies of the bound states become undisturbed, which are equal to the initial values, after the laser field is turned off. Now, we focus on the ground state indicated by the green dashed curves in Fig. 5. Generally, the ground-state energy is lower in the external laser pulse. Thus, the effective ionization potential in the Coulomb explosion process becomes larger, resulting in the energy shift in the JES observed in Fig. 3(a). In detail, as the nuclear energy increases, the amplitude of the oscillation decreases, which is consistent with the tendency of the energy shift in the JES observed in Fig. 3(a). In Figs. 5(c) and 5(d), for $6 < t < 10$ fs, the faint blue color extending down to $E = -1$ a.u. can be observed. These populations denote the highly excited states of H_2^+ dressed by the external laser field. The energies of these highly excited states shift as well under the influence of the laser pulse. Additionally, a similar calculation is performed for the model atom. Figure 6 shows the time evolution of the electron wave packet of bound states of the model atom with ionization energies corresponding to Figs. 5(a)–5(i), respectively. One can see that the oscillation of energy of the ground state is very slight for the atom. The energy shift can be ignored, as is observed in Fig. 4. Therefore, the counterintuitive distribution is attributed to the significant Stark shift in strong fields.

According to Ref. [32], the Stark shift of the ground state a is proportional to $F V_{ka}$. V_{ka} is the dipole matrix element coupling the ground state a with the first excited state k and it can be calculated by $\langle \Psi_k | x | \Psi_a \rangle$. In our simulation, the electric field F varies very slowly and the dipole matrix element V_{ka} plays the major role in the process. The values of V_{ka}, which are determined by the potential energy structure, of the H_2^+ molecule are much larger compared with the atom. Therefore, the influence of the Stark effect on the H_2^+ molecule is more significant. In Fig. 7, we present the dipole coupling matrix element V_{ka} of H_2^+ molecule for the ground state $1s\sigma_g$ and the first excited state $2p\sigma_u$ as a function of the nuclear energy E_N. V_{ka} decreases as the nuclear energy increases, which is consistent with the variation of oscillation amplitude of the ground-state energy in Fig. 5.

To quantitatively analyze the energy shift in the JES, we now investigate the electronic ATI spectra of H_2^+ in two different nuclear energies. The energy shift of the ground state of the H_2^+ molecule can be expressed by [32]

$$\Delta E = V_g(R) - \frac{V_g(R) + V_u(R)}{2} + \sqrt{\frac{[V_g(R) - V_u(R)]^2}{4} + [F(t)V_{ka}(R)]^2}, \quad (9)$$
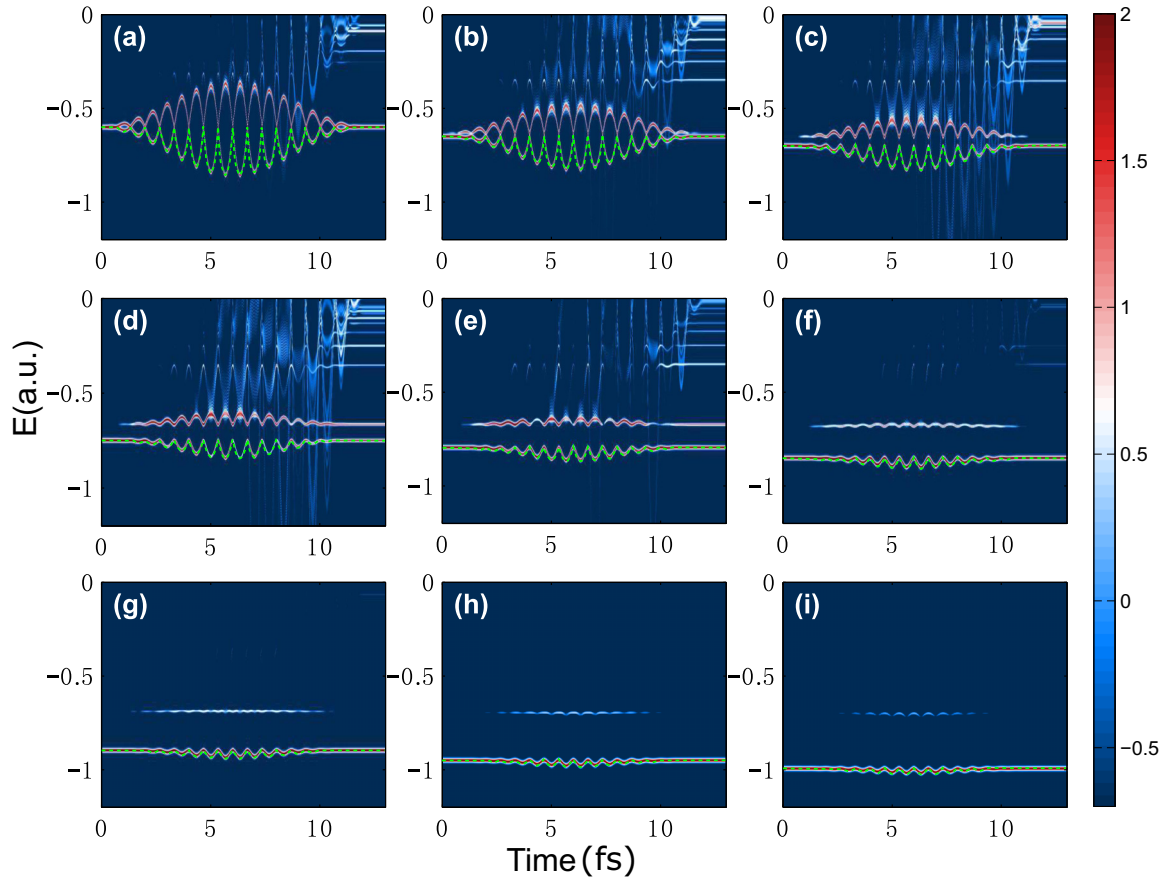
FIG. 5. The time evolution of the electron wave packet of bound states of H_2^+ for different nuclear energies. In (a)–(i), $E_N = 0.1, 0.144, 0.182, 0.217, 0.25, 0.29, 0.323, 0.364, 0.4$ a.u., respectively. The color scale is logarithmic and in arbitrary units.
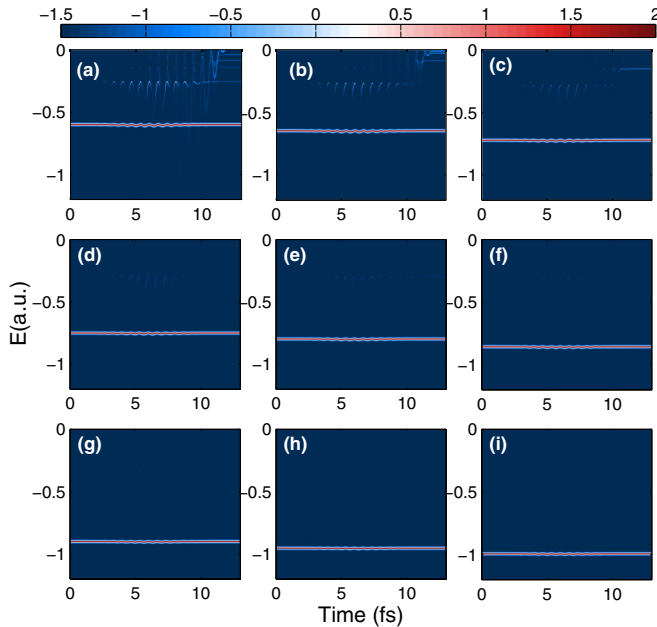

FIG. 6. The time evolution of the electron wave packet of bound states of the model atom with ionization energies corresponding to Figs. 5(a)–5(i), respectively. The color scale is logarithmic and in arbitrary units.

where V_g and V_u are the potential curves of the ground state $1s\sigma_g$ and the first excited state $2p\sigma_u$, respectively, and $F(t)$ is the instantaneous electric field. From Figs. 3(b) and 3(c), we "read" the energy shifts $\Delta E_1 = 0.07$ a.u. and $\Delta E_2 = 0.11$ a.u. by $\Delta E_i = Et_i - Er_i$, where Et_i is the energy calculated by Eq. (1) and Er_i is the peak value of the ATI, corresponding to the internuclear distances of $R = 4$ a.u. and $R = 5.5$ a.u., respectively. Here, the photon number absorbed in the process
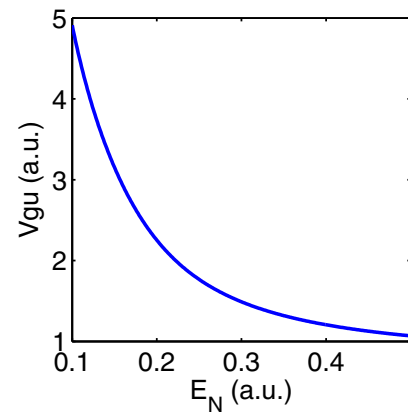

FIG. 7. Dipole coupling matrix element V_{ka} for the two lowest electronic states of the H_2^+ molecule.
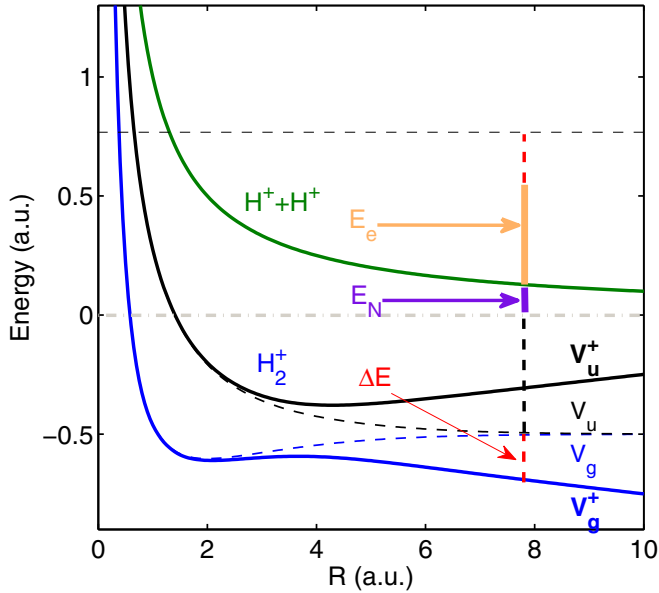
FIG. 8. Illustration of electron–nuclear-energy sharing including the Stark effect in the Coulomb explosion process of the H_2^+ molecule. See text for details.

n is 11. We have tested that the energy shifts for different multiphoton peaks are the same. Then, by applying Eq. (9), we obtain the energy shifts of the ground state of the H_2^+ molecule $\Delta E_1' = 0.06$ a.u. and $\Delta E_2' = 0.1$ a.u., which are in good agreement with the values in Figs. 3(b) and 3(c). As to the time t in Eq. (9), we use the time $t = 5.7$ fs, when the amplitude of the laser field has the maximum, because at this instant the electron has a maximum ionization probability.

The electron–nuclear-energy sharing that includes the Stark effect of molecules is illustrated in Fig. 8. V_g^+ and V_u^+ are the field-dressed potential curves and they are calculated by $[V_g(R) + V_u(R)]/2 \mp \sqrt{[(V_g(R) - V_u(R))^2]/4 + [F(t)V_{ka}(R)]^2}$. Obviously, the field-dressed potential curve of the ground state V_g^+ is lower than the field-free potential curve V_g due to the Stark effect. The energy shift of the ground state is ΔE, as indicated by the red dashed vertical line in Fig. 8. The analytical solution of ΔE can be obtained by Eq. (9). In Fig. 8, the dashed vertical lines below the gray dotted-dashed horizontal lines indicate the part of the energy that the H_2^+ molecule needs to overcome in the above-threshold multiphoton ionization, while the solid vertical lines show the part that remained after the laser pulse is off. Compared to Fig. 1, the part of the energy that needs to be overcome in ionization becomes larger resulting from the Stark shift. The electronic energy E_e has to compensate for the part of the shift energy ΔE induced

by the Stark effect, as indicated in Fig. 8. Therefore, the electronic energy E_e is reduced in the process, resulting in the energy shifts in the JES as shown in Fig. 3(a). Consequently, the energy-sharing rule including the Stark effect in the Coulomb explosion process of the H_2^+ molecule can be given by $E_e = n\omega + V_g - 1/R - U_p - \Delta E$ and $E_N = 1/R$. As is seen in Fig. 8, the energy shift of the ground state ΔE increases as the internuclear distance extends to larger R. From Eq. (9), one can see that ΔE is a function of R. Thus, the internuclear distance may be reconstructed from the energy shifts of the JES in the above-threshold multiphoton ionization, which will be of vital importance for molecular structure imaging using strong laser fields.

IV. CONCLUSION

In conclusion, the electron–nuclear-energy sharing of H_2^+ subjected to a 400-nm laser pulse has been theoretically studied by solving the TDSE. By analyzing the JES quantitatively, we found a counterintuitive energy shift, which becomes more pronounced for lower nuclear energies. To uncover the origin of the energy shifts, we compare the electronic ATI spectra for the H_2^+ molecule and a hydrogenlike model atom with the same ionization potential. We show the energy shifts of the H_2^+ molecule are much larger with respect to the atom. Then, by tracing the time evolution of the electron wave packets of the bound states, clear Stark shift of the ground-state energy of the H_2^+ molecule is observed. This reveals that the energy shift in the JES is caused by the Stark effect, which is induced by the strong coupling of the two lowest-lying states of H_2^+ in the strong laser fields. Furthermore, we have calculated the Stark-induced shift with an analytic method, which is in good agreement with the *ab initio* result. Experimentally, this shift might be observed in the future, e.g., by a pump-probe technology [33]. By changing the time delay between the pump and probe pulses, the internuclear separation of the H_2^+ molecule at which the ionization takes place can be controlled. The JES offers a wealth of information about the ultrafast electron and nuclear dynamics of the molecules, which could provide an alternative approach to detect molecular structure and ultrafast electron dynamics in molecules.

[1] J. L. Krause, K. J. Schafer, and K. C. Kulander, Phys. Rev. Lett. **68**, 3535 (1992).

[2] T. Zuo, S. Chelkowski, and A. D. Bandrauk, Phys. Rev. A **48**, 3837 (1993).

[3] O. Smirnova, Y. Mairesse, S. Patchkovskii, N. Dudovich, D. Villeneuve, P. Corkum, and M. Y. Ivanov Nature (London) **460**, 972 (2009).

[4] L. He, P. Lan, Q. Zhang, C. Zhai, F. Wang, W. Shi, and P. Lu, Phys. Rev. A **92**, 043403 (2015); J. Luo, Y. Li, Z. Wang, Q. Zhang, and P. Lu, J. Phys. B **46**, 145602 (2013).

[5] V. Roudnev, B. D. Esry, and I. Ben-Itzhak, Phys. Rev. Lett. **93**, 163601 (2004).

[6] M. F. Kling, C. Siedschlag, A. J. Verhoef, J. I. Khan, M. Schultze, T. Uphues, Y. Ni, M. Uiberacker,

M. Drescher, F. Krausz, and M. J. Vrakking, Science **312**, 246 (2006).

[7] N. G. Kling, K. J. Betsch, M. Zohrabi, S. Zeng, F. Anis, U. Ablikim, B. Jochim, Z. Wang, M. Kübel, M. F. Kling, K. D. Carnes, B. D. Esry, and I. Ben-Itzhak, Phys. Rev. Lett. **111**, 163004 (2013).

[8] Z. Wang, K. Liu, P. Lan, and P. Lu, Phys. Rev. A **91**, 043419 (2015); P. Lan, E. J. Takahashi, K. Liu, Y. Fu, and K. Midorikawa, New J. Phys. **15**, 063023 (2013); K. Liu, Q. Zhang, P. Lan, and P. Lu, Opt. Express **21**, 5107 (2013); K. Liu, Q. Zhang, and P. Lu, Phys. Rev. A **86**, 033410 (2012).

[9] X. Y. You and F. He, Phys. Rev. A **89**, 063405 (2014).

[10] H. Stapelfeldt, E. Constant, and P. B. Corkum, Phys. Rev. Lett. **74**, 3780 (1995).

[11] B. D. Esry, A. M. Sayler, P. Q. Wang, K. D. Carnes, and I. Ben-Itzhak, Phys. Rev. Lett. **97**, 013003 (2006).

[12] T. Zuo and A. D. Bandrauk, Phys. Rev. A **52**, R2511 (1995).

[13] N. Takemoto and A. Becker, Phys. Rev. Lett. **105**, 203004 (2010).

[14] Y. Zhou, C. Huang, Q. Liao, and P. Lu, Phys. Rev. Lett. **109**, 053004 (2012); A. Tong, Y. Zhou, and P. Lu, Opt. Express **23**, 15774 (2015).

[15] I. Sánchez and F. Martín, Phys. Rev. Lett. **79**, 1654 (1997).

[16] F. Martín, J. Fernández, T. Havermeier, L. Foucar, T. Weber, K. Kreidi, M. Schöffler, L. Schmidt, T. Jahnke, O. Jagutzki, A. Czasch, E. P. Benis, T. Osipov, A. L. Landers, A. Belkacem, M. H. Prior, H. Schmidt-Böcking, C. L. Cocke, and R. Dörner, Science **315**, 629 (2007).

[17] C. B. Madsen, F. Anis, L. B. Madsen, and B. D. Esry, Phys. Rev. Lett. **109**, 163003 (2012).

[18] R. E. F. Silva, F. Catoire, P. Rivière, H. Bachau, and F. Martín, Phys. Rev. Lett. **110**, 113001 (2013).

[19] L. Yue and L. B. Madsen, Phys. Rev. A **88**, 063420 (2013).

[20] K. Liu, P. Lan, C. Huang, Q. Zhang, and P. Lu, Phys. Rev. A **89**, 053423 (2014).

[21] L. Yue and L. B. Madsen, Phys. Rev. A **90**, 063408 (2014).

[22] V. Mosert and D. Bauer, Phys. Rev. A **92**, 043414 (2015).

[23] J. Ullrich, R. Moshammer, A. Dorn, R. Dörner, L. P. H. Schmidt, and H. Schmidt-Böcking, Rep. Prog. Phys. **66**, 1463 (2003).

[24] J. Wu, M. Kunitski, M. Pitzer, F. Trinter, L. P. H. Schmidt, T. Jahnke, M. Magrakvelidze, C. B. Madsen, L. B. Madsen, U. Thumm, and R. Dörner, Phys. Rev. Lett. **111**, 023002 (2013).

[25] B. Feuerstein and U. Thumm, Phys. Rev. A **67**, 043405 (2003).

[26] A. Staudte, D. Pavičić, S. Chelkowski, D. Zeidler, M. Meckel, H. Niikura, M. Schöffler, S. Schössler, B. Ulrich, P. P. Rajeev, Th. Weber, T. Jahnke, D. M. Villeneuve, A. D. Bandrauk, C. L. Cocke, P. B. Corkum, and R. Dörner, Phys. Rev. Lett. **98**, 073003 (2007).

[27] Z. Wang, K. Liu, P. Lan, and P. Lu, J. Phys. B **48**, 015601 (2015).

[28] K. Liu, Q. Li, P. Lan, and P. Lu, Mol. Phys. **113**, 3247 (2015).

[29] Y. Li, P. Lan, H. Xie, M. He, X. Zhu, Q. Zhang, and P. Lu, Opt. Express **23**, 28801 (2015).

[30] K. J. Schafer and K. C. Kulander, Phys. Rev. A **42**, 5794 (1990).

[31] M. Li, P. Zhang, S. Luo, Y. Zhou, Q. Zhang, P. Lan, and P. Lu, Phys. Rev. A **92**, 063404 (2015).

[32] T. Y. Xu and F. He, Phys. Rev. A **90**, 053401 (2014).

[33] H. Xu, F. He, D. Kielpinski, R. T. Sang, and I. V. Litvinyuk, arXiv:1504.04676.